Modeling and performance of a metamaterial beam with magnetically coupled resonators

Shuo Wang[a], Chunbo Lan[a*], Guobiao Hu[b], Yabin Liao[c]

[a]College of Aerospace Engineering, Nanjing University of Aeronautics and Astronautics, Nanjing 210016, China

[b]Internet of Things Thrust, The Hong Kong University of Science and Technology (Guangzhou), Guangzhou, Guangdong 511400, China

[c]Department of Aerospace Engineering, Embry-Riddle Aeronautical University--Prescott, Prescott, AZ, USA

ABSTRACT

During the past decade, structural nonlinearities have been utilized to widen the bandgaps of locally resonant metamaterials. In this paper, a novel metamaterial beam with nonlinear coupled oscillators as its local resonator is developed to enlarge the low-frequency bandgaps. First, the governing equations of the magnetically coupled metamaterial beam are established based on the Euler-Bernoulli theory. Subsequently, the transmittance and bandgap properties of such a nonlinear metamaterial beam are studied. It is revealed that by increasing the coupled nonlinear stiffness effectively broadens the low-frequency bandgap. A parametric study is conducted to ascertain the effects of critical parameters, such as coupled nonlinear stiffness, base excitation, and the difference between the two coupled local oscillators, on the bandgaps and vibration suppression performance. It is observed that the coupled nonlinear stiffness has a significant impact on the transmittance of metamaterial beams, while the resonant frequency difference has a relatively minor influence on the transmittance. Meanwhile, the bandgap will shift to high-frequency range as the base excitation increases. Several useful conclusions are summarized and provided as guidelines for further structural optimization and performance enhancement.

Keywords: nonlinear metamaterial; low-frequency bandgap; magnets; vibration suppression.

1. INTRODUCTION

In recent years, local resonance metamaterials have experienced rapid development and have emerged as an effective approach for low-frequency vibration reduction in structural applications. Local resonance acoustic metamaterials can be primarily categorized into linear and nonlinear types. Typical linear models include single-cell structures with either a single-degree-of-freedom local resonator or multiple local resonators within a single cell. Researchers have utilized these fundamental models to design structures aimed at broadening the bandgap [1−3]. However, linear acoustic metamaterials still face significant challenges, such as substantial additional mass and limited effectiveness in reducing vibrations only at frequencies matching the local resonance. Consequently, there is a pressing need to develop feasible methods that can overcome these limitations and achieve low-frequency, broadband, lightweight, and efficient vibration suppression.

Active and Passive Smart Structures and Integrated Systems XIX, edited by Xiaopeng Li, Yangyang Chen, Guoliang Huang, Mostafa A. Nouh, Christopher Sugino, Serife Tol, Jinkyu Yang, Proc. of SPIE Vol. 13432, 1343203 · © 2025 SPIE · 0277-786X · doi: 10.1117/12.3051199

Nonlinear acoustic metamaterials have emerged as a promising research direction within the broader field of metamaterials [4-8]. Nonlinear models can be categorized into three primary types: both the local resonators and the main chain exhibit nonlinearities; only the main chain exhibits nonlinearity while the local resonators is linear; and only the local resonators exhibit nonlinearity while the main chain is linear [9]. Utilizing these nonlinear models, researchers can design a variety of nonlinear acoustic metamaterials. Moreover, nonlinearity introduces unique characteristics, such as amplitude-dependent bandgaps [10], chaotic bands [6], adaptive bands [11], and high-order harmonics [12]. The incorporation of nonlinear effects into acoustic metamaterials holds the potential to significantly broaden low-frequency bandgaps and enhance vibration reduction performance with minimal additional mass. Zhang S et al. [13] designed a novel asymmetric beam incorporating a series of Duffing resonators. Frequency response analysis was performed using the harmonic balance method and validated through finite element simulations. The results demonstrated that adjusting the linear or nonlinear stiffness could effectively tune the bandgap range. Moreover, introducing softening nonlinearity resulted in an ultra-wide bandgap, which was nearly three times wider than the linear bandgap. Xue Y et al. [14] introduced a new type of spring-lever-MRE nonlinear local resonant metamaterial. When the excitation amplitude was set to 10^{-5} mm and the lever ratio increased from 1 to 4, the bandgap range shifted from 290.4 Hz - 481.7 Hz to 36.3 Hz - 60.1 Hz, achieving broadband vibration attenuation at extremely low frequencies.

Despite significant advancements, broadening the bandgap at low frequencies remains a challenge for nonlinear acoustic metamaterials. To explore additional methods for enhancing low-frequency bandgaps, this paper proposes a novel coupled nonlinear metamaterial beam and analyzes its behavior using nonlinear inner coupling. The main contents of this paper are as follows: Section 2 derives the equations of motion for the coupled nonlinear metamaterial beam; Section 3 examines the transmittance of the beam and the influence of various parameters; Section 4 summarizes the key findings.

2. MATHEMATICAL MODELING

Figure 1 illustrates the finite-length model of the coupled nonlinear metamaterial beam. The main beam has a length L and is equipped with S unit cells, each spaced at a constant interval d_1 along its length. Within each unit cell, two local resonators are positioned at a distance d_2 apart. To minimize mutual interference between adjacent unit cells, d_1 should significantly larger than d_2. For convenience, the two local resonators within each unit cell are named as LR 1 and LR 2. The mass, stiffness, and damping coefficients of LR 1 are denoted as m_1, k_1, and c_1, respectively; those for LR 2 are m_2, k_2, and c_2, respectively. The two local resonators are interconnected via a nonlinear spring. The left end of the beam is clamped, and base excitation $w_b(t) = W_b e^{i\omega t}$ is applied at this fixed end, characterized by a base acceleration $A_{cc} = -\omega^2 W_b$.

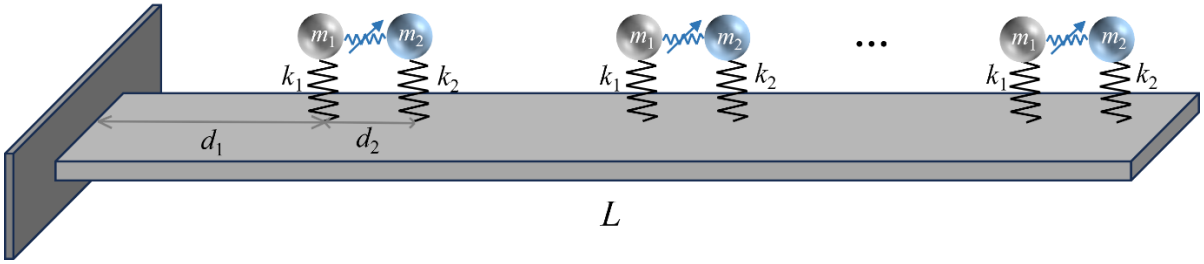

Figure 1 Finite-length model of the coupled nonlinear metamaterial beams

Based on Euler-Bernoulli beam theory, the governing equation for the coupled nonlinear metamaterial beam can be written

as

$$EI\frac{\partial^4 w_{rel}(x,t)}{\partial x^4}+c_s I\frac{\partial^5 w_{rel}(x,t)}{\partial x^4\partial t}+\rho A_{cs}\frac{\partial^2 w_{rel}(x,t)}{\partial t^2}=\rho A_{cs}A_{cc}e^{iwt}-\sum_{j=1}^{S}\left[F_j^1\delta\left(x-x_j^1\right)+F_j^2\delta\left(x-x_j^2\right)\right]e^{i\omega t} \tag{1}$$

where $w(x,t)$ is the absolute displacement of the main beam at position x , $w_{rel}(x,t)$ is the displacement of the main beam relative to the foundation， $w_{rel}(x,t) = w(x,t) - w_b(t)$. EI, ρ and A_{cs} are the bending stiffness, density and cross-section area of the host beam, respectively. c_s is the equivalent strain rate damping constant. F_j^1 and F_j^2 are the reaction forces exerted by LR 1 and LR 2 in the jth cell onto the beam, respectively; $\delta(x)$ is the Dirac delta function.

The governing equations of LR 1 and LR 2 at jth cell are given as:

$$\begin{cases} m_1\ddot{u}_j^1(t)+c_1\dot{u}_j^1(t)+k_1u_j^1(t)+k_c\left(u_j^1(t)+w\left(x_j^1,t\right)-u_j^2(t)-w\left(x_j^2,t\right)\right)+k_3\left(u_j^1(t)+w\left(x_j^1,t\right)-u_j^2(t)-w\left(x_j^2,t\right)\right)^3=-m_1\ddot{w}(x_j^1,t) \\ m_2\ddot{u}_j^2(t)+c_2\dot{u}_j^2(t)+k_2u_j^2(t)+k_c\left(u_j^2(t)+w\left(x_j^2,t\right)-u_j^1(t)-w\left(x_j^1,t\right)\right)+k_3\left(u_j^2(t)+w\left(x_j^2,t\right)-u_j^1(t)-w\left(x_j^1,t\right)\right)^3=-m_2\ddot{w}(x_j^2,t) \end{cases} \tag{2}$$

where, u_j^1 and u_j^2 are the displacements of LR 1 and LR 2 relative to the host beam in jth cell. k_c is the coupled linear stiffness, k_3 is the coupled nonlinear stiffness.

Using the modal superposition method, the relative displacement along the beam can be written as

$$w_{rel}(x,t)=\sum_{k=1}^{\infty}\phi_k(x)\eta_k(t)\quad(k=1,2,3...) \tag{3}$$

where functions $\phi_k(x)$ are the normalized mode shape functions of the plain beam and functions $\eta_k(t)$ are the modal coordinates.

Substituting Eq. (3) into Eq. (1), multiplying by $\phi_n(x)$, and integrating over the beam length from zero to L, using the orthogonal conditions, the modal governing equation is obtained as:

$$\ddot{\eta}_n(t)+2\zeta_n\omega_n\dot{\eta}_n(t)+\omega_n^2\eta_n(t)=\rho A_{cs}a_{cc}e^{i\omega t}\int_0^L\phi_n(x)dx-\sum_{j=1}^{S}\left[F_j^1\phi_n\left(x_j^1\right)e^{i\omega t}+F_j^2\phi_n\left(x_j^2\right)e^{i\omega t}\right] \tag{4}$$

where $\zeta_n = c_sI\omega_n/(2E)$.

By solving Eq. (4), the modal coordinates can $\eta_n(t)$ be obtained. Substituting the coordinates back to Eq. (3), the host beam's deflection can be obtained as

$$w_{rel}(x,t)=\sum_{k=1}^{\infty}\phi_k(x)\frac{\rho A_{cs}a_{cc}\int_0^L\phi_k(x)dx-\sum_{j=1}^{S}\left[F_j^1\phi_k\left(x_j^1\right)+F_j^2\phi_k\left(x_j^2\right)\right]}{\omega_k^2-\omega^2+2i\zeta_k\omega_k\omega}e^{i\omega t} \tag{5}$$

The reverse force of LR 1 and LR 2 can be represented by:

$$\begin{cases} F_j^1=-\left[c_1\dot{u}_j^1(t)+k_1u_j^1(t)\right] \\ F_j^2=-\left[c_2\dot{u}_j^2(t)+k_2u_j^2(t)\right] \end{cases} \tag{6}$$

The transmittance of the host beam is

$$T_r = 20\log\left(\frac{|w_{rel}(L) + w_b|}{|w_b|}\right) \tag{7}$$

3. TRANSMITTANCE AND PARAMETRIC STUDY

3.1 Transmittance

To conduct a preliminary investigation of the transmittance of coupled nonlinear metamaterial beams, the governing equations were numerically solved using the fourth-order Runge-Kutta method. The frequency sweep rate was set to 0.01 Hz/s, and the base excitation amplitude was 0.1 m/s². Frequency sweep simulations were performed using the parameters listed in Table 1.

Table 1 Structural Parameters of Nonlinearly Internally Coupled Metamaterial Beams

Parameter	Value	Parameter	Value
Equivalent mass, m_1 [g]	10	Equivalent mass, m_2 [g]	5
Equivalent damping coefficient, c_1 [N·m/s]	2.3×10^{-4}	Equivalent damping coefficient, c_2 [N·m/s]	1.8×10^{-4}
Equivalent stiffness, k_1 [N/m]	246.49	Equivalent stiffness, k_2 [N/m]	315.5
Linear coupling stiffness, k_c[N/m]	-35	Nonlinear coupling stiffness, k_3[N/m^3]	35×10^4
Beam length, L [m]	0.47	Beam width, b [m]	0.02
Beam thickness, h [m]	0.001	Beam density, ρ [kg/m^3]	7860
Beam Young's modulus, E	200×10^9	Number of oscillators, S	10
Distance of unit cell, d_1 [mm]	56	Distance of resonators d_2 [m]	38

Figure 2 illustrates the transmittances of the linear configuration and that of the coupled nonlinear metamaterial beam with a coupled nonlinear stiffness k_3 of 35×10^4 N/m³. It is shown that the linear configuration exhibits two bandgaps 24.90Hz–31.12Hz and 38.60Hz–57.40Hz. After introducing nonlinear inner coupling, these bandgaps shift to 22.80Hz–27.16Hz and 36.50Hz–57.40Hz, respectively. For the first bandgap, both the starting and cutoff frequencies shift towards lower frequencies, resulting in a bandwidth reduction of 1.86 Hz. The second bandgap's cutoff frequency remains constant at 57.40 Hz, while its starting frequency decreases from 38.60 Hz to 36.50 Hz, increasing the bandwidth from 18.9 Hz to 21.0 Hz. In summary, the introduction of coupled nonlinear makes the bandgaps shift towards lower frequencies and broadens the second bandgap.

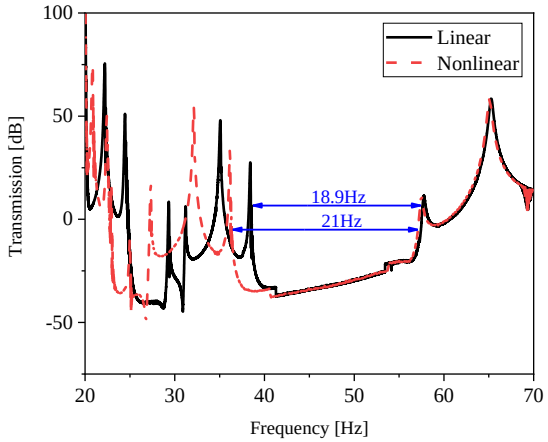

Figure 2 Transmittance of the uncoupled linear and coupled nonlinear metamaterial beam(k_3=35×10^{4}N/m^3)

3.2 Parametric study

As demonstrated in the previous section, the introduction of coupled nonlinear can effectively broaden the low-frequency bandgap. In this section, we will further investigate the effects of parameters, including coupled nonlinear stiffness, base excitation amplitude, and the natural frequencies of the two local resonators within a unit cell, on the transmittance of the metamaterial beam.

3.2.1 Effect of coupling stiffness

Figure 3 illustrates the transmittance of the metamaterial beam for coupled nonlinear stiffnesses of 15 × 10^4 N/m^3, 25 × 10^4 N/m^3, and 35 × 10^4 N/m^3. As discussed in the previous section, the linear configuration exhibits two bandgaps 24.90Hz–31.12Hz and 38.60Hz–57.40Hz. After introducing nonlinear internal coupling, when the stiffness is set to 15 × 10^4 N/m^3, the bandgap ranges shift to 24.13Hz–29.50Hz and 37.50Hz–57.40Hz. Bandgap 1 shifts towards lower frequencies, with its bandwidth decreasing by 0.85 Hz; the cutoff frequency of bandgap 2 remains unchanged, while its starting frequency decreases from 38.60 Hz to 37.50 Hz, expanding the entire bandgap range from 18.90 Hz to 20.00 Hz, an increase of 1.1 Hz. When the coupled nonlinear stiffness increases to 25 × 10^4 N/m^3, bandgap 1 continues to shift towards lower frequencies, changing its range to 23.40 Hz to 28.40 Hz, resulting in a bandwidth reduction of 1.22 Hz compared to the linear configuration. The cutoff frequency of bandgap 2 remains constant, while its starting frequency decreases from 38.60 Hz to 37.00 Hz, expanding the entire bandgap range from 18.90 Hz to 20.50 Hz, an increase of 1.6 Hz. Finally, when the coupled nonlinear stiffness reaches 35 × 10^4 N/m^3, both the starting and cutoff frequencies of bandgap 1 shift towards lower frequencies, reducing the bandwidth by 1.86 Hz. The cutoff frequency of bandgap 2 remains unchanged, while its starting frequency decreases from 38.60 Hz to 36.50 Hz, expanding the bandgap from 18.9 Hz to 21 Hz, an increase of 2.1 Hz.

In summary, the introduction of nonlinear internal coupling results in the following changes as the coupled nonlinear stiffness gradually increases: the cutoff frequency of bandgap 1 shifts progressively towards lower frequencies, and its bandwidth narrows; the cutoff frequency of bandgap 2 remains constant, while its starting frequency shifts progressively towards lower frequencies, leading to an expansion of its bandwidth. Consequently, the addition of coupled nonlinear enables the broadening of the low-frequency bandgap.

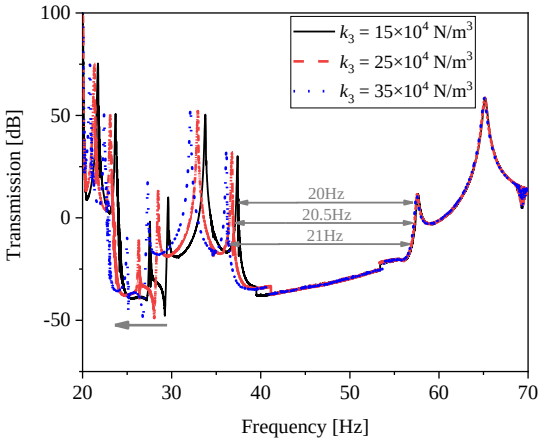

Figure 3 Transmittance of the metamaterial beam for different coupled nonlinear stiffnesses

3.2.2 Effect of base excitation

Subsequently, the influence of base excitation on the transmittance of the metamaterial beam with a coupled nonlinear stiffness of 15 × 10^4 N/m³ is analyzed, as shown in Figure 4. The results indicate that when the base excitation amplitude A_{cc} = 0.1 m/s², the minimum transmission loss for the two bandgaps are -39.20 dB and -37.52 dB, respectively. When the base excitation increases to A_{cc} = 0.3 m/s², the cutoff frequency of bandgap 1 remains unchanged, while its starting frequency shifts towards higher frequencies, resulting in a bandwidth reduction from 5.27 Hz to 4.77 Hz. Additionally, the minimum transmission loss for bandgap 1 decreases from -39.20 dB to -46.34 dB, and for bandgap 2, it decreases from -37.52 dB to -52.12 dB . When the base excitation further increases to 0.5 m/s², the starting frequency of bandgap 1 continues to shift towards higher frequencies, reducing the bandgap range from 5.27 Hz to 4.11 Hz. The minimum transmission loss for both bandgaps decrease to -49.18 dB and -61.37 dB, respectively. In summary, as the base excitation increases, the bandwidth of bandgap 1 decreases and shifts towards higher frequencies, while the minimum transmission loss for both bandgaps also decrease.

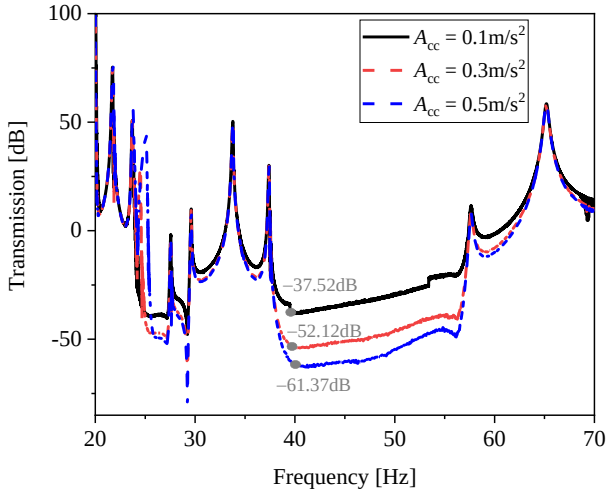

Figure 4 Transmittance of the metamaterial beam for different base excitations

3.2.3 Effect of the intrinsic frequency of local resonators

Finally, the impact of the natural frequencies of the two local resonators within a unit cell on the transmittance is investigated. As illustrated in Figure 5(a), when the natural frequencies of LR 1 and LR 2 are set to 25 Hz and 35 Hz respectively, the linear configuration exhibits bandgap ranges of 24.89 Hz - 29.95 Hz and 34.20 Hz - 52.30 Hz. After introducing a coupled nonlinear stiffness of 15×10^4 N/m³, the bandgap ranges shift to 24.20 Hz - 28.20 Hz and 33.20 Hz - 52.30 Hz. Consequently, the bandwidth of bandgap 1 decreases by 1.06 Hz, while that of bandgap 2 increases by 1 Hz. When the natural frequencies of LR 1 and LR 2 are set to 25 Hz and 40 Hz respectively, the linear configuration exhibits bandgap ranges of 24.90 Hz - 31.12 Hz and 38.60 Hz - 57.40 Hz. After introducing the same coupled nonlinear stiffness, the bandgap ranges change to 24.13 Hz - 29.50 Hz and 37.50 Hz - 57.40 Hz. The bandwidth of bandgap 1 decreases by 0.85 Hz, while that of bandgap 2 increases by 1.1 Hz. When the natural frequencies of LR 1 and LR 2 are set to 25 Hz and 50 Hz respectively, the linear configuration exhibits bandgap ranges of 24.83 Hz - 32.77 Hz and 47.00 Hz - 68.80 Hz. After introducing the coupled nonlinear stiffness, the bandgap ranges change to 24.10 Hz - 31.12 Hz and 46.00 Hz - 68.80 Hz. The bandwidth of bandgap 1 decreases by 0.92 Hz, while that of bandgap 2 increases by 1 Hz. In summary, the natural frequencies of the local resonators have a relatively minor influence on the overall transmittance of the coupled nonlinear metamaterial beam.

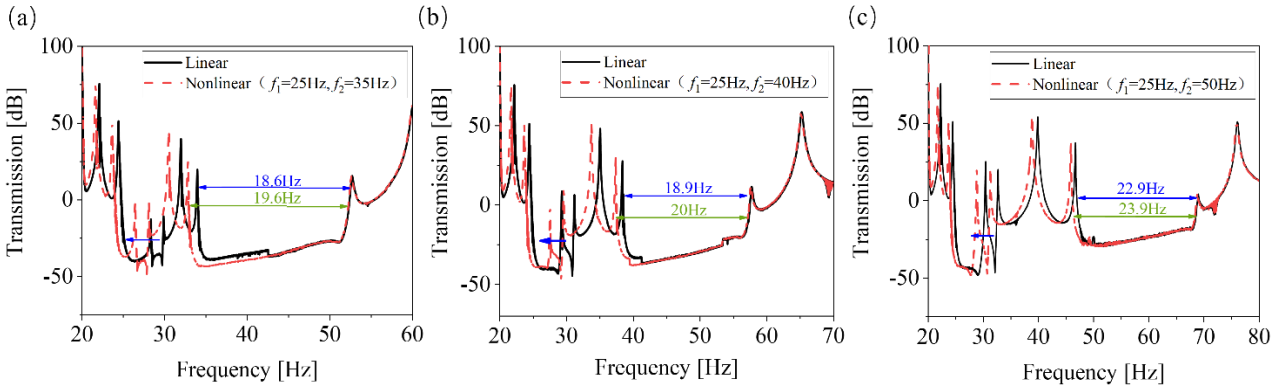

Figure 5 Transmittance of the metamaterial beam for different LR intrinsic frequency

4. CONCLUSIONS

This study investigates a coupled nonlinear metamaterial beam. The governing equations for the metamaterial beam and its resonators are derived, followed by an initial analysis of the transmittance using numerical simulations. Subsequently, the effects of coupled nonlinear stiffness, base excitation, and the natural frequencies of the two local resonators within a unit cell on the transmittances are examined.

The following conclusions are drawn:

(1) Compared with the linear configuration, after adding nonlinear coupling, the bandgap 1 shifts towards low frequency and its bandwidth narrows; the cutoff frequency of the bandgap 2 remains unchanged, but its starting frequency shifts towards low frequency and its bandwidth increases.

(2) Parameter analysis reveals that the coupled nonlinear stiffness has the most significant impact on the transmittance of

the metamaterial beam. In contrast, the natural frequencies of the two local resonators within a unit cell have a relatively minor influence. Increasing the coupling stiffness results in a broader bandgap range for the bandgap 2. Therefore, employing a higher coupled nonlinear stiffness can effectively broaden the low-frequency bandgap.

ACKNOWLEDGEMENT

This study was financially supported by the Funds of National Key Laboratory of Helicopter Aeromechanics (Grant No. 2024-CXPT-GF-JJ-093-04), the Fundamental Research Funds for the Central Universities (Grant No. NT2024002), National Natural Science Foundation of China (Grant No. 52305135), Guangzhou Municipal Science and Technology Project (Grant No. 2023A03J0011), Guangdong Provincial Key Lab of Integrated Communication, Sensing and Computation for Ubiquitous Internet of Things (Grant No. 2023B1212010007), and Guangzhou Municipal Key Laboratory on Future Networked Systems (Grant No. 024A03J0623).

REFERENCES

[1] Wang, G., Wen, X., Wen, J., Liu, Y., "Quasi-one-dimensional periodic structure with locally resonant band gap," Journal of Applied Mechanics., 73(1):167-170(January 2006). http://dx.doi.org/10.1115/ 1.2061947

[2] Hu, G., Tang, L., Das, R., Gao, S., Liu, H., "Acoustic metamaterials with coupled local resonators for broadband vibration suppression," AIP Advances., 7(2), 025211(1 February 2017). http://dx.doi.org/10.1063/1.4977559

[3] Celli, P., Yousefzadeh, B., Daraio, C., Gonella, S., "Bandgap widening by disorder in rainbow metamaterials," Applied Physics Letters., 114(9), 091903(4 March 2019). http://dx.doi.org/10.1063/1.5081916

[4] Fang, X., Wen, J., Yin, J., Yu, D., "Wave propagation in nonlinear metamaterial multi-atomic chains based on homotopy method," AIP Advances., 6(12), 121706(1 December 2016). http://dx.doi.org/10.1063/1.4971761

[5] Fang, X., Wen, J., Yin, J., Yu, D., Xiao, Y., "Broadband and tunable one-dimensional strongly nonlinear acoustic metamaterials: Theoretical study," Physical Review E., 94(5), 052206(2016). http://dx.doi.org/10.1103/PhysRevE.94.052206

[6] Fang, X., Wen, J., Bonello, B., Yin, J., Yu, D., "Wave propagation in one-dimensional nonlinear acoustic metamaterials," New Journal of Physics., 230:4453-4461(26 September 2019). http://dx.doi.org/10.1007/s00707-019-02514-8

[7] Fang, X., Wen, J., Bonello, B., Yin, J., Yu, D., "Ultra-low and ultra-broad-band nonlinear acoustic metamaterials," 8(1), 1288(1 December 2017). http://dx.doi.org/10.1038/s41467-017-00671-9

[8] Khajehtourian, R., Hussein, M. I., "Dispersion characteristics of a nonlinear elastic metamaterial," AIP Advances., 4(12):124308(22 December 2014). http://dx.doi.org/10.1063/1.4905051

[9] Fang, X., Lacarbonara, W., Cheng, L., "Advances in nonlinear acoustic/elastic metamaterials and metastructures," Nonlinear Dynamics., (2024). http://dx.doi.org/10.1007/s11071-024-10219-4

[10] Gong, C., Fang, X., Cheng, L., "Band degeneration and evolution in nonlinear triatomic metamaterials," Nonlinear Dynamics., 111(1):97-112(January 2023). http://dx.doi.org/10.1007/s11071-022-07860-2

[11] Fang, X., Wen, J., Benisty, H., Yu, D., "Ultrabroad acoustical limiting in nonlinear metamaterials due to adaptive-broadening band-gap effect," 101(10), 104304(1 March 2020). http://dx.doi.org/10.1103/PhysRevB.101.104304

[12] Zhang, J., Romero-García, V., Theocharis, G., Richoux, O., Achilleos, V., Frantzeskakis, D., “Second-Harmonic Generation in Membrane-Type Nonlinear Acoustic Metamaterials,” Crystals., 6(8), 86(August 2016). http://dx.doi.org/ 10.3390/cryst6080086

[13] Zhang, S., Lou, J., Fan, H., Du, J., “A nonlinear acoustic metamaterial beam with tunable flexural wave band gaps,” Engineering Structures., 276, 115379(1 February 2023). http://dx.doi.org/10.1016/j.engstruct.2022.115379

[14] Xue, Y., Li, J., Wang, Y., Song, Z., Krushynska, AO., “Widely tunable magnetorheological metamaterials with nonlinear amplification mechanism,” International Journal of Mechnical Sciences., 264, 108830(15 February 2024). http://dx.doi.org/10.1016/j.ijmecsci.2023.108830

[15] Zhang, J., Zhang, J., Zhang, B., An, Y., Yang, X., Hu, N., Ma, L., Peng, Y., Wang, B., “Broadband multifrequency vibration attenuation of an acoustic metamaterial beam with two-degree-of-freedom nonlinear bistable absorbers,” Mechanical Systems and Signal Processing., 212, 111264(15 April 2024). http://dx.doi.org/ 10.1016/j.ymssp.2024.111264

[16] Fronk, M., Fang, L., Packo, P., Leamy, M., “ Elastic wave propagation in weakly nonlinear media and metamaterials: a review of recent developments,” Nonlinear Dynamics., 111(12):10709-10741(June 2023). http://dx.doi.org/ 10.1007/s11071-023-08399-6

[17] Deng, B., Wang, P., He, Q., Tournat, V., Bertoldi, K., “Metamaterials with amplitude gaps for elastic solitons,” Nature Communication., 9(1), 3410(1 December 2018). http://dx.doi.org/10.1038/s41467-018-05908-9

[18] Hu, G., Tang, L., Baneriee, A., Das, R., “Metastructure With Piezoelectric Element for Simultaneous Vibration Suppression and Energy Harvesting,” Journal of vibration and acoustics, 139(1), 011012(1 February 2017). http://dx.doi.org/10.1115/1.4034770

[19] Liu, Y., Yu, D., Li, L.,Zhao, H., Wen, J., Wen, X., “Design guidelines for flexural wave attenuation of slender beams with local resonators,” Physics Letters., 362(5-6):344-347(12 March 2007). http://dx.doi.org/10.1016/j.physleta.2006.10.056

[20] Gao, N., Wu, J H., Hou, H., Yu, L., “Excellent low-frequency sound absorption of radial membrane acoustic metamaterial,” International Journal of Modern Physics B, 31(3), 1750011(30 January 2017). http://dx.doi.org/ 10.1142/S0217979217500114